# Effects of temperature and pH on uniform and pitting corrosion of aluminium alloy 6061-T6 and characterisation of the hydroxide layers

Sarah L'haridon-Quaireau, Mathilde Laot, Kimberly Colas, Bénédicte Kapusta, Sylvie Delpech, Dominique Gosset

# Journal Pre-proof


Effects of temperature and pH on uniform and pitting corrosion of aluminium alloy 6061-T6 and characterisation of the hydroxide layers

Sarah L'Haridon-Quaireau, Mathilde Laot, Kimberly Colas, Bénédicte Kapusta, Sylvie Delpech, Dominique Gosset

PII: S0925-8388(20)31509-7

DOI: https://doi.org/10.1016/j.jallcom.2020.155146

Reference: JALCOM 155146

To appear in: *Journal of Alloys and Compounds*

Received Date: 23 January 2020

Revised Date: 26 March 2020

Accepted Date: 10 April 2020

Please cite this article as: S. L'Haridon-Quaireau, M. Laot, K. Colas, Béé. Kapusta, S. Delpech, D. Gosset, Effects of temperature and pH on uniform and pitting corrosion of aluminium alloy 6061-T6 and characterisation of the hydroxide layers, *Journal of Alloys and Compounds* (2020), doi: https://doi.org/10.1016/j.jallcom.2020.155146.

Sarah L'HARIDON-QUAIREAU: Investigation, Methodology, Conceptualization, Writing – original draft, Review and editing

Mathilde LAOT: Investigation

Kimberly COLAS : Supervision, Validation, Review and editing

Bénédicte KAPUSTA: Funding acquisition, Project administration

Sylvie DELPECH: Supervision, Validation, Conceptualization

Dominique GOSSET: Methodology,

# Effects of temperature and pH on uniform and pitting corrosion of aluminium alloy 6061-T6 and characterisation of the hydroxide layers

Sarah L'HARIDON-QUAIREAU, Mathilde LAOT, Kimberly COLAS, Bénédicte KAPUSTA,
DEN-Service d'Etude des Matériaux Irradiés, CEA, Université Paris-Saclay
F-91191, Gif-sur-Yvette – France

Sylvie DELPECH
IJCLab, Paris-Saclay University
Paris - France

Dominique GOSSET
DEN-Service de Recherche de Métallurgies Appliquées, CEA, Université Paris-Saclay
*F-91191, Gif-sur-Yvette - France*

Corresponding author: S. L'HARIDON-QUAIREAU, sarah.quaireau@laposte.net



## HIGHLIGHTS:

- Uniform corrosion film of hydroxide aluminium shows a layered structure.
- At 70°C, the film is composed of different aluminium hydroxide phases.
- Corrosion of magnesium present in the alloy causes pH increase in deaerated medium.
- Corrosion of iron-rich particles passivate pits.

## ABSTRACT:

During operation in material testing reactors (MTR), the AA-6061-T6 alloy used for core components is covered by aluminium hydroxide. In this work we investigate the effects of parameters on pitting and uniform corrosion of the aluminium alloy 6061-T6 in the conditions found in MTR for the core structures: temperature (70-100°C) and pH (5 and 7.5). After corrosion experiments, characterisation techniques are used to observe the formed hydroxide, its composition and crystallographic structure (TEM, SEM, EDX, XRD, µ-Raman spectroscopy and electron diffraction) and formulate hypotheses on

alloy. In addition, corrosion models are used to predict the hydroxide thickness in MTR for a safe and efficient operation. These models are based on empirical correlations. The data obtained from this study allows to discuss the application of these models at low temperature (70°C).



## KEYWORDS:

Aluminium hydroxide; Corrosion; Microstructure; pH.

## 1. INTRODUCTION

Due to low activation, good neutron transparency and good mechanical properties, the aluminium alloy AA-6061-T6 is used in Materials Testing Reactors (MTRs) for the structures of nuclear core and for fuel cladding [1–3]. In MTRs, the coolant is typically nitric acid diluted in pure water in order to obtain a pH between 5 and 6 [4,5]. The maximum temperature reached for the core structures outside of the fuel elements is typically between 70 and 100°C [6]. In these conditions, the aluminium alloy is corroded and a film of aluminium hydroxide covers the surface of the alloy. Since the thermal conduction of this hydroxide is low (~2 W/m/K [7]), the film degrades heat exchanges between the core structures and the coolant. It could therefore lead to an overheating of the core [3]. As a result, it is important to quantify growth of the film for safe and efficient operation of MTRs. In this regard, some empirical models were developed to predict the thickness of the film. They are based on empirical correlations between hydroxide thicknesses, testing time and corrosion conditions (pH, temperature, heat flux and flow rate) [1,8,9]. All the models have the same form:

$X_{ox} = X_0 + k*t^p$

Where $X_{ox}$ and $X_0$ are the oxide thicknesses and t the time ($X_0$ is the thickness at t=0). The coefficients p and k depend on pH, temperature, heat flux and flow rate. Depending on the observations done during corrosion tests, they are adjusted using data obtained after corrosion tests at high temperature, above 100°C [1,2,4,5,8,10,11]. At a temperature above 80°C, the main crystalline phase of aluminium hydroxide is boehmite (γ-AlOOH) [7,12]. However, part of the core structures in MTR are at a lower temperature, below 70°C, where the main hydroxide phase is bayerite (α-$Al(OH)_3$). This change of hydroxide phase at 70/80°C has an effect on the corrosion of aluminium according to Hart [13]. As a result, new quantitative measurements are required at low temperature (70°C) to complete the data in order to improve the application ranges of the empirical models. In this work, a parametric study has been performed on the aluminium alloy AA-6061-T6: different values of temperature and pH are tested. In order to highlight the impact of the change of the aluminium hydroxide phases at 70/80°C on aluminium corrosion, two temperatures are tested in this work: 70 and 100°C. Furthermore, the hydroxide thickness prediction models found in the literature [1,8,14] depend on the pH of the corrosion solution. As a result, in order to complete the data for these empirical correlations, different values of pH are tested at 70°C: 5 and 7.5

surrounding the iron-rich inclusions: pits of aluminium hydroxide are observed in the alloy [17]. The micrometric $Mg_2Si$ particles have anodic behaviour: they are preferentially corroded protecting the aluminium matrix from oxidation [18]. In this work, measurements are done to quantify the uniform corrosion and the micrometric localised corrosion. For these two types of corrosion, the corrosion product obtained at low temperature (70°C) is characterised using various techniques in order to better understand the effect of temperature and pH on 6061-T6 alloy corrosion. Its microstructure is observed by SEM and TEM. Its crystalline structure is studied using Selected Area Electron Diffraction (SAED) performed in a TEM, µ-Raman, and X-rays diffraction (XRD). Its chemical composition is studied by Energy Dispersive X-rays spectrometry (EDX). In addition to micrometric precipitates, nanometric phases are present in the 6061-T6 alloy [21–23], their corrosion behaviour is the subject of several studies [24,25] and thus is not studied in this work.

## 2. EXPERIMENTAL METHODS AND SAMPLES

During this study, corrosion tests are performed in autoclave in order to investigate the influence of various parameters on pitting and uniform corrosion of an Al-Mg-Si aluminium alloy for nuclear applications. The conditions of these experiments are described in Table 1. Two temperatures are tested: 70 and 100°C. Two pH are tested: 5 and 7.5. However, pH variations are observed in the smaller volume of solution tested (0.065L). As a result, a larger volume of solution (2.8L) is used in order to highlight the impact of pH variations on aluminium corrosion. The 2.8L volume reduces pH variations by an effect of dilution. This section describes the samples and autoclaves used in this study. A description of the type of examinations performed on the corroded samples is also given.

Table 1: Conditions (temperature, pH and solutions) of the corrosion tests performed in this study

| Studied parameter | Temperature | Corrosive solution | Volume of solution |
|---|---|---|---|
| Temperature | 70-100°C | Initial pH: 6 (nitric acid diluted in pure water) | 0.065L |
| pH | 70°C | Average pH: 5 and 7.5(nitric acid diluted in pure water) | 0.065L and 2.8L |

*Samples and preparation:*

The samples are AA6061-T6 aluminium alloy. This alloy's main elements are Al (balance), Fe (0.7%mass), Si (0.4-0.8 %mass), Cu (0.15-0.4%mass) and Mg (0.8-1.2%mass). The samples are coupon-shaped with dimensions of 10 mm x 20 mm x 1.4 mm. The T6 treatment was obtained by solution annealing at 550°C for 4h following by water quenching and tempering at 175°C for 4h. This treatment allows to improve the mechanical characteristic [26]. The grain size is 180 µm on average.

µm and 1 µm. All samples are then cleaned with ethanol and dried. For each corrosion test, three samples are corroded together in the same solution. As a result, the points on the curves presented in Fig 9.a and b represent the average of measurements performed on three samples (The data joined to the article is also about the average data measured on three samples: the average thicknesses and the average mass gains). For each corrosion duration studied, three new samples are used in order to avoid opening the autoclave during the experiment. Indeed it has been observed in literature that interruptions during corrosion tests can artificially limit aluminium corrosion [3].

*Autoclaves:*

In order to perform the corrosion tests, two autoclaves are used. The autoclaves are in 316L steel. The inside is covered with polytetrafluoroethylene in order to avoid contamination of the samples surface by iron from the autoclave. The sample holder is in zirconium alloy in order to limit galvanic coupling between aluminium alloy samples and the sample holder. Before performing the corrosion tests, helium is injected in the autoclave in order to deoxygenate the corrosive media. The pressure in the autoclave is imposed by the vapour pressure (i.e. the pressure is 0.5 bar relative at 70°C).

*Solutions:*

The solutions used for corrosion are obtained by dilution of concentrated nitric acid with distilled water in order to obtain an initial pH of 5 and 6. Before and after each corrosion experiment, the pH of the solution is measured with the pH-meter *PH1001* from *VWR* Company (the evolution of pH during the test is however not monitored in-situ). Chemical composition of solutions before and after each test is determined by Inductively Coupled Plasma Atomic Emission Spectroscopy (ICP-AES, equipment: *Optima 2000 DV* model from *Perkin Elmer* Company). In particular, measurement of aluminium, silicon, iron and magnesium concentrations are performed.

*Examinations after corrosion tests:*

After corrosion, samples are cut in half. The first half of each sample is used for surface examinations (microstructure). The second half is embedded in a conductive resin at ambient temperature and polished down to a 1µm finish with diamond paste in order to examine the cross section of the samples. This embedded part is used for examinations with Scanning Electron Microscopy (SEM, *iT300* model from *JEOL*) and Optical Microscopy (OM, *GX 51* model from *Olympus*).

Different measurements are performed on the corroded samples to quantify pitting and uniform corrosion. The thickness of the film is measured on the samples' cross-section. For each sample, five micrographs of the film are taken at different positions with a SEM. The thickness of the film is measured on these micrographs using the *ANALYSIS™* software: 100 measurements are performed on each micrograph. The average of these 500 measurements is taken as a result.

Pits of aluminium hydroxide are characterized using OM. The depth of pits is measured on the cross section of the embedded samples when a precipitate responsible of the formation of this pit (the iron-rich precipitate) is observed in the centre of the pit near the corroded surface of the sample. An

on Fig. 1). The embedded samples are polished several times on about several millimetres to allow measurement of about 150 different pits. Then the average depth of these 150 measurements is taken as a result and is presented in Fig. 9.a.

The crystalline phases of the hydroxide are studied using low-incidence X-ray diffraction (XRD) and µ-Raman spectroscopy. The X-rays diffractometer (*CPS120 –Curved Position Sensitive- detector from INEL*) is used with Cu-Kα1 radiation (Ge(111) monochromator, wavelength: 1.5406 Ă) in an asymmetric configuration. The incident angle of the X-ray beam is 2°: in this configuration, the analysed depth is about 3 µm in Al metal and 5 µm in the hydroxides. The µ-Raman spectrometer (*InVia Reflex* from *Reinshaw)* is used with a green laser (wavelength: 532 nm) and at 5% of the spectrometer power (5% of 100mW, to limit hydroxide damage during the analyses). The µ-Raman analyses are performed on the cross-section of the embedded samples with an optical microscope with a magnification of 50x.

To characterize the hydroxide film at the nanoscale, Transmission Electron Microscopy is used (TEM: *TECNAI 3042* model from *FEI*, with an acceleration voltage of 200 kV and a length camera of 865 mm). TEM samples of the corroded materials are prepared with conventional Focused Ion Beam (FIB: *Auriga 40* model from *ZEISS*) methods. A Pt deposit is added to the samples' surface to protect the hydroxide layer during the TEM thin film preparation.



## 3. RESULTS

### 3.1 CHARACTERISATION OF THE CORROSION PRODUCT AT 70°C

Two families of micrometric precipitates are present in the 6061-T6 alloy: the iron-rich inclusions and the $Mg_2Si$ particles. These two micrometric precipitates cause localised corrosion. Their corrosion behaviour is presented in this section. The film associated to uniform corrosion is also characterised. No intergranular corrosion has been observed in the samples studied here (MEB and TEM observations).

#### 3.1.1 Corrosion behaviour of the micrometric iron–rich intermetallics

Pits of aluminium hydroxide are observed: concave pits of boehmite (γ-AlOOH) are present in the aluminium matrix (Fig. 1, aluminium hydroxide analysed by µ-Raman analyses which are described in the next part). On the top of concave pits of boehmite, a pile of bayerite crystals (α-$Al(OH)_3$, analysed by µ-Raman) is present: the pits are also visible on the surface of the samples. These pits are due to galvanic coupling between the micrometric iron-rich inclusions and the aluminium matrix [16]. Fig. 1 presents a cross section of a typical pit obtained after corrosion at 70°C, for 30 days in 2.8L of solution at a constant pH of 5. In the SEM micrograph, two large iron-rich inclusions are present in the concave pit. The corroded inclusion N°2, in the centre of the pit, causes the formation of the pit. This inclusion N°2 contains oxygen and iron according to the EDX maps of Al, Fe and O presented in Fig. 1. The non-corroded inclusion N°1, in contact with the aluminium matrix, causes a local increase of the depth

inclusion. Selective aluminium dissolution during the corrosion of Fe-containing inclusions had already been observed in the literature [28].

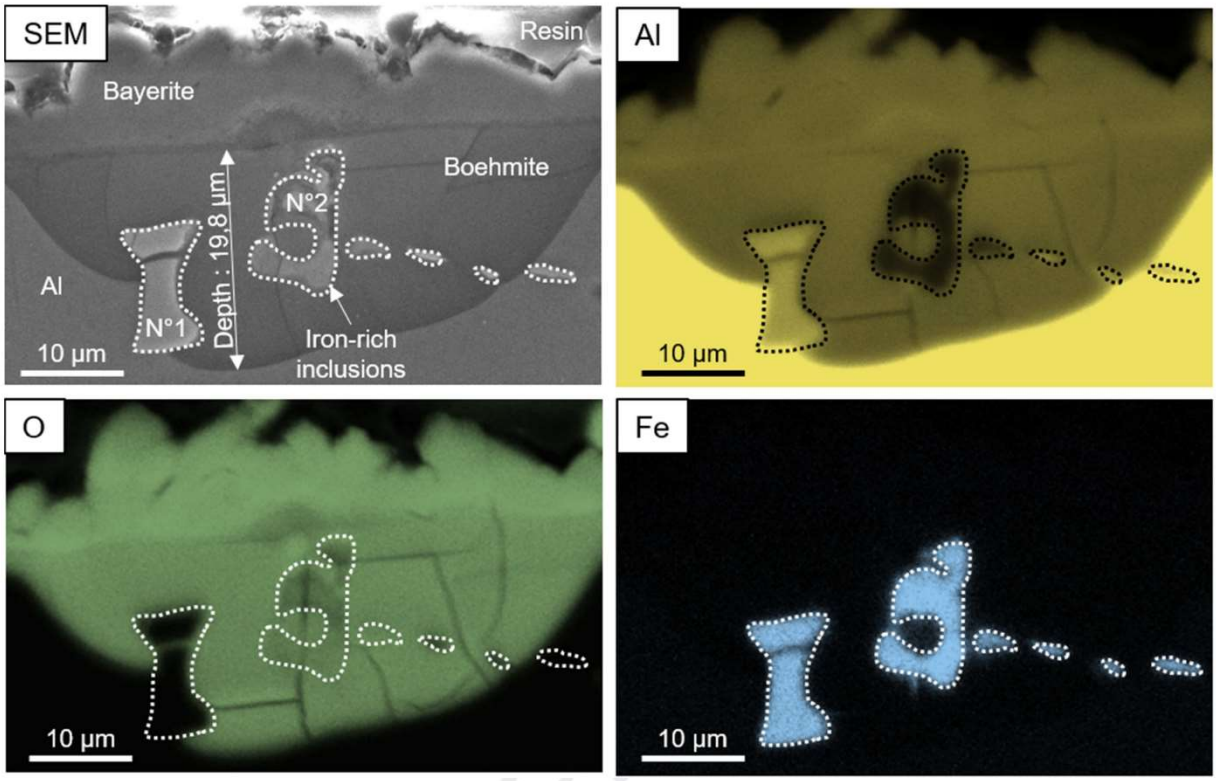


Figure 1: Micrograph of an aluminium hydroxide pit (SEM, secondary electron mode) and the corresponding dispersive X-rays spectroscopy of Al, O and Fe obtained after corrosion test at 70°C, for 30 day and in 2.8L of solution at pH 5.

In addition, µ-Raman analysis is performed on an inclusion located in the centre of a pit like the inclusion N°2 in Fig. 1 in order to investigate its crystalline structure. Fig. 2 presents the pattern obtained from this analysis. Peaks of this Raman pattern are attributed to magnetite ($Fe_3O_4$) [29]. The peak at 350-360 $cm^{-1}$ is the main peak of boehmite [30] and is due to the boehmite surrounding the precipitate. The formation of magnetite ($Fe_3O_4$) at a pH of 5 is not in accordance to the iron Pourbaix diagram: indeed at 25°C, at a pH of 5, the stable form of oxidised iron is the aqueous ion $Fe^{3+}$ [31]. In this study, iron is not detected in solution after corrosion tests. Linnenbom indicated that at 60°C, in a neutral solution without dissolved dioxygen, oxidised iron tended to form magnetite instead of aqueous ion [32]. In this study, before corrosion tests, the dioxygen present in the atmosphere and in the solution is removed by injecting helium in autoclaves. The stability of magnetite is thus due to the absence of dioxygen in the corrosive medium. Park et al. indicated that micrometric iron-rich inclusions caused the formation of pits in the aluminium matrix [16]. This study shows that after the formation of pits, the emerging iron-rich inclusions are corroded: there is dissolution of aluminium and formation of a solid iron oxide.

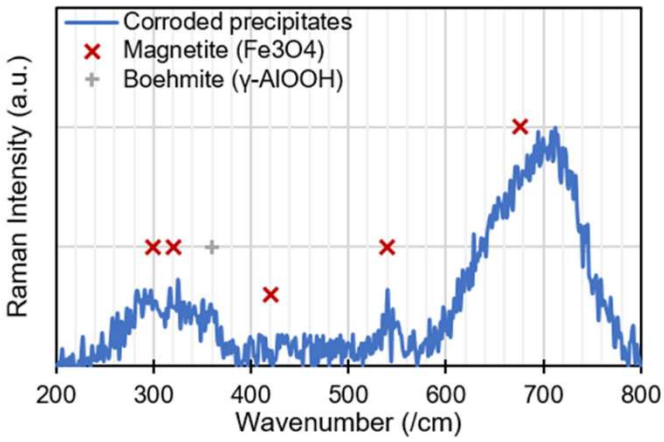


Figure 2: μ-Raman pattern of an iron-rich inclusion located in the centre of an aluminium hydroxide pit, obtained after corrosion test at 70°C, for 30 day and in 2.8L of solution at pH 5.

### 3.1.2 Corrosion behaviour of the micrometric $Mg_2Si$ particles

The micrometric $Mg_2Si$ particles exhibit an anodic corrosion behaviour: they are preferentially corroded in the aluminium matrix. Fig. 3 presents a cross section of $Mg_2Si$ particles observed in the aluminium matrix. On this picture, the particle in contact with the hydroxide film is corroded: oxygen is present in the particle and a selective dissolution of the magnesium is observed in the corroded area of the particle. These observations are in accordance with the Pourbaix diagram of magnesium [31] which predicted that, in neutral aqueous medium, the stable form of magnesium is the aqueous ion $Mg^{2+}$. This ion does not form complex with hydroxyl group and the solubility of magnesium in solution is very high: the magnesium is released in solution. During the corrosion of Mg-containing particles in aluminium alloys, selective dissolution of magnesium is common [19,20,24]. The stable form of silicon is the solid phase $SiO_2$ in neutral aqueous medium in the corresponding Pourbaix diagram [31], the chemical composition of the corroded $Mg_2Si$ particles is in accordance to this Pourbaix diagram: after the corrosion of the particle, this is composed of a mix of silicon and oxygen. When the $Mg_2Si$ are fully corroded, since the oxidized silicon and magnesium are in a stable form according to their corresponding Pourbaix diagram [31], it is expected that the fully-corroded $Mg_2Si$ do not play a major role on aluminium alloy corrosion

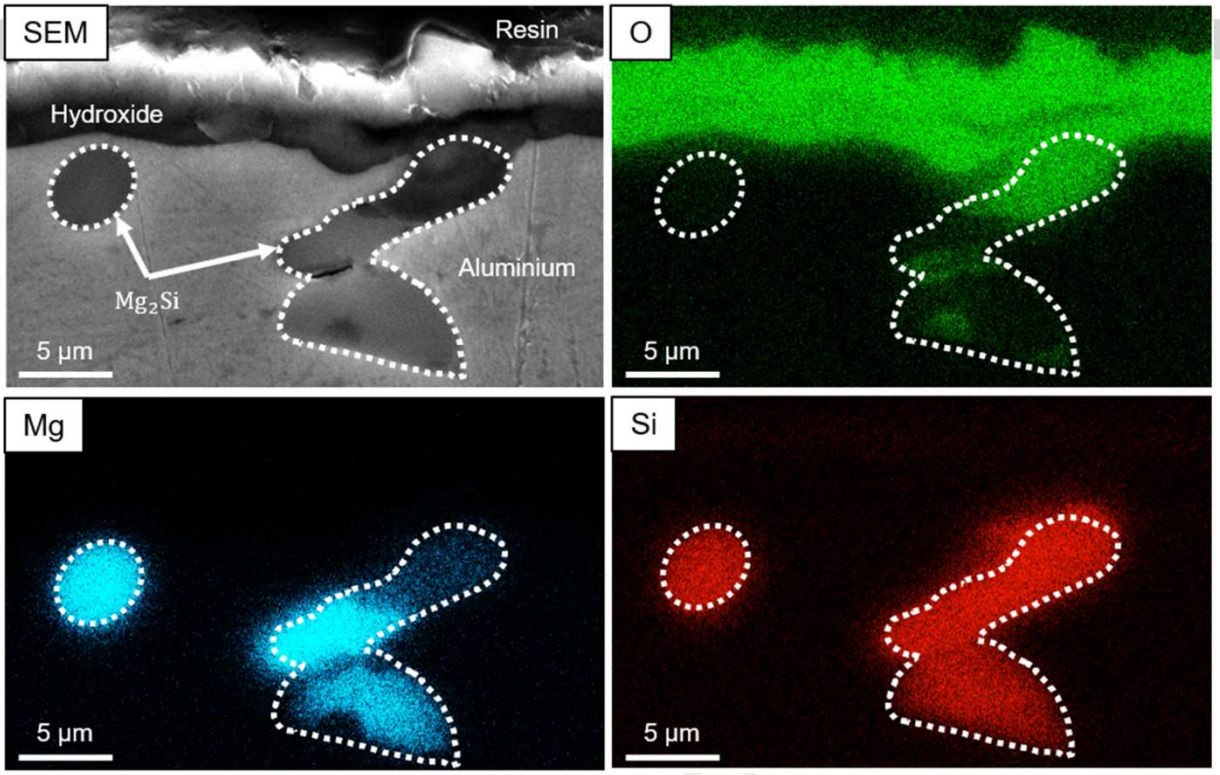


Figure 3: Micrograph of $Mg_2Si$ particles (SEM, secondary electron mode) and corresponding dispersive X-rays spectroscopy of O, Mg and Si obtained after corrosion test at 70°C, for 30 day and in 2.8L of solution at pH 5.

### 3.1.3 Aluminium hydroxide film associated to uniform corrosion

A relatively uniform film of aluminium hydroxide covers the surface of the samples. Fig. 4.a present a cross section of the film observed with a TEM. This film was obtained after a corrosion test at 70°C for 10 days in 2.8L of solution at a constant pH of 5. The film is composed of three layers: an inner, an intermediate and an outer layer. To characterise the hydroxide at 70°C, microanalyses are performed on each layer: µ-Raman analysis and/or electron diffraction.

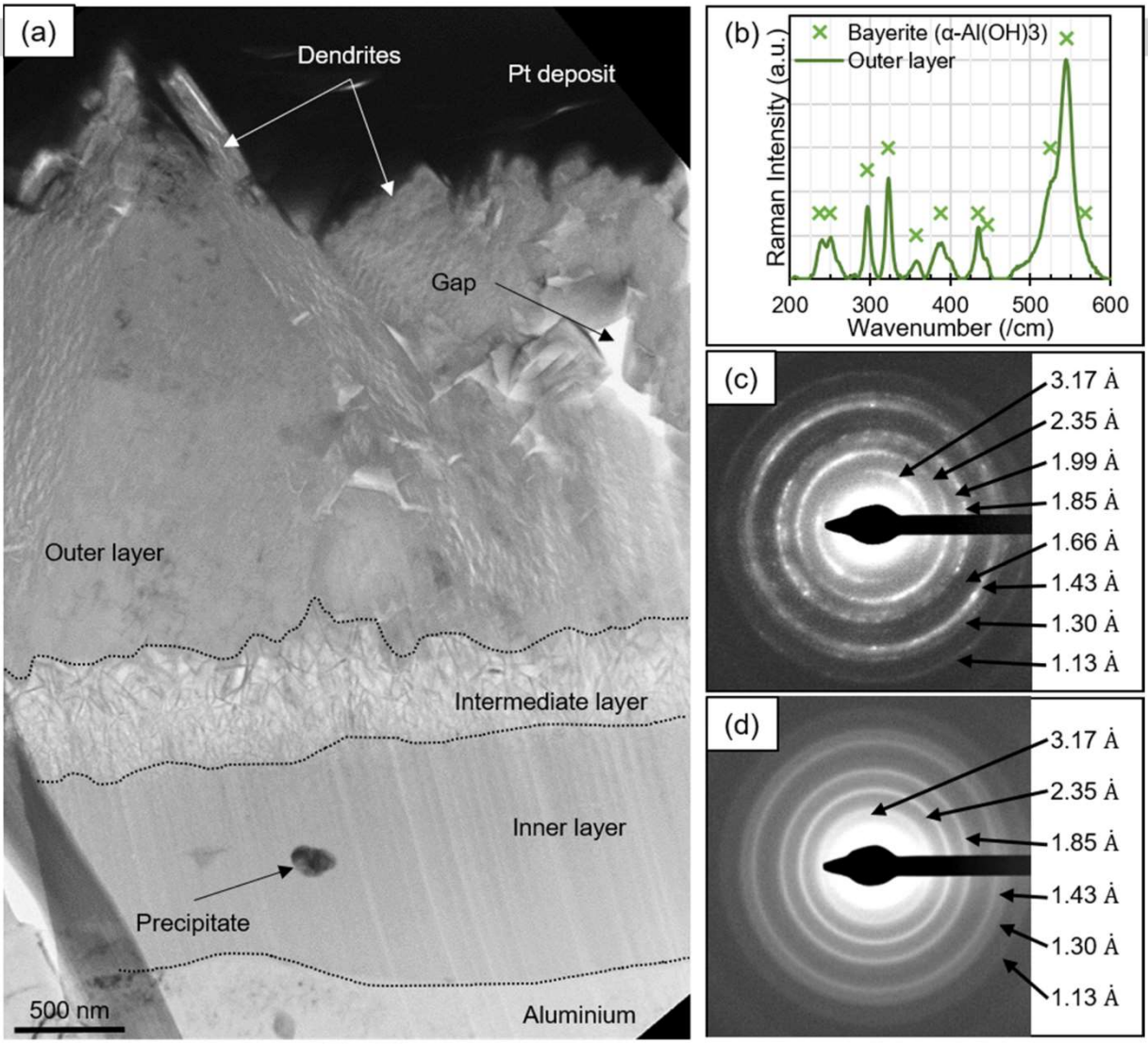


Figure 4: (a) Micrograph of a cross section of the aluminium hydroxide film in bright field imaging (TEM), (b) μ-Raman pattern obtained on the the outer layer, and selected area electron diffraction patterns obtained from (c) the intermediate layer and (d) the inner layer (TEM); obtained after corrosion at 70°C, for 10 days in 2.8L of solution at a constant pH value of 5.

The outer layer is composed of micro-sized crystals. The size of these microcrystals is between 0.3 and 3 μm. This layer is porous as gaps are present between the micron-sized crystals. A μ-Raman analysis indicates this layer is fully crystallised bayerite (α-$Al(OH)_3$): the measured emission bands correspond to the ones of this hydroxide [33] as shown in Fig. 4.b.The presence of this hydroxide at 70°C is in accordance with the phase diagram of aluminium hydroxide of Wefers and Misra [12].
The inner layer in contact with the metal is compact as illustrated in Fig. 4.a. The intermediate layer is composed of needle-shaped nanocrystallites as shown in Fig. 4.a. SAED is performed on these two layers, the electron diffraction patterns are presented in Fig. 4.b and c. The two layers are composed of boehmite (γ-AlOOH): the d-spacing measured at 3.17Å, 2.35Å, 1.99Å, 1.85Å, 1.66Å, 1.43Å, 1.30Å

layer, the nanocrystallites are not well defined and appear below the ten nanometer scale, in the intermediate layer, the length of the needle-shaped nanocrystallites is at most 200 nm (Fig. 4.a). However, the presence of boehmite at 70°C is not in accordance with the phase diagram of aluminium hydroxide: according to Wefers and Misra [12], only bayerite should be present at 70°C, thus, boehmite is metastable. In addition, the micrometric precipitates do not change the layered microstructure and the crystalline composition of the aluminium hydroxide: μ-Raman analyses were performed at several points in aluminium hydroxide pit.

The film of aluminium hydroxide was characterised at 250°C by Wintergerst et al. [3]: the authors showed that the film was composed of two layers: an inner layer and an outer layer, both were composed of boehmite. The inner layer grows internalyand the outer layer grows externaly (this layer grew by aluminium ion precipitation) [3]. This study shows that at 70°C, a thin intermediate layer is also observed between the two main layers and, the inner layer and the outer layer are not composed of the same phase of aluminium hydroxide. Bayerite (outer layer) and boehmite (inner layer) have not the same properties (density, hydration, solubility) [12]. Thus, these two layers could have different behaviour (dissolution, growth) depending on the parameters of corrosion (pH, temperature). As a result, a parametric study with different temperatures and pH is performed in this study.

## 3.2 PARAMETRIC STUDY

The parametric study presented in this section focuses on the impact of temperature and pH on uniform and pitting corrosion of the aluminium alloy AA-6061-T6.

### 3.2.1 Influence of the temperature on aluminium corrosion

In order to better understand the impact of the change of aluminium hydroxide phase on aluminium corrosion, two corrosion tests are performed in autoclave at 70°C and 100°C. For 33 days, aluminium samples are corroded in aqueous media with an initial pH of 6. The volume of solution is 0.065L. After corrosion tests, the pH of the solutions is 6.8.

The mass gain of the three samples is on average 146.8 ± 0.4 mg/dm² at 70°C and 48.2 ± 0.3 mg/dm² at 100°C. The total thickness of the hydroxide film is on average 4.9 ± 0.2 μm at 70°C and on average 1.5 ± 0.2 μm at 100°C. The pits of aluminium hydroxide in the metal are deeper at 70°C than at 100°C: their average deep is 21.3 ± 0.9 μm at 70°C and 12.5 ±1.2 μm at 100°C. As a result, the samples are more corroded at 70°C than at 100°C. This observation is similar to the one made by Hart during corrosion tests performed at 60 and 80°C [13].

X-rays diffraction analyses (XRD) are performed on the corroded samples at 70 and 100°C. The patterns obtained from these analyses are presented in Fig. 5. The XRD peak positions are compared to those found in the American Mineralogist Crystal Structure Database (AMCSD) [36] for boehmite (γ-AlOOH, Card No. 0020685 in AMCSD) [35], bayerite (α-$Al(OH)_3$, Card No. 0010649 in AMCSD) [37] and aluminium (Card No. 0011136 in AMCSD) [38]. The peaks associated with aluminium on the XRD patterns are due to the aluminium matrix of the samples. The main hydroxide crystalline phase at

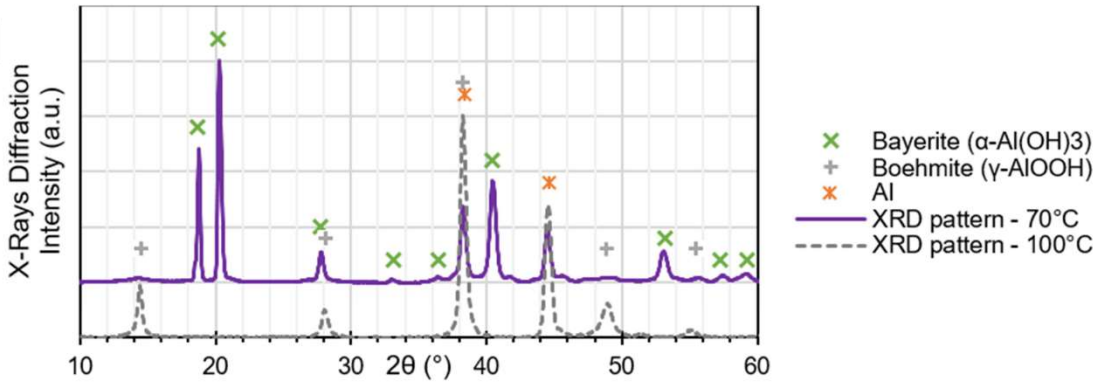


Figure 5: X-ray diffraction patterns obtained on the corroded samples surface at 70 and 100°C, for 33 days of corrosion and in 0.065L of solution at initial pH 6.

During the corrosion process, aluminium is released in solution from the dissolution of the metal matrix. The aluminium concentration in the solution is measured after the corrosion tests by ICP-AES: it is about $(4.95 \pm 0.7)*10^{-6}$ mol/L at 70°C and $(3.1 \pm 0.6)*10^{-6}$ mol/L at 100°C, for a final pH of 6.8. These measured concentrations can be compared to the calculated solubility of boehmite and bayerite. Chivot [39] calculated the solubility of these hydroxides in pure water. For his calculation, the author considered the following species: $Al^{3+}$, $Al(OH)^{2+}$, $Al(OH)_2^{+}$, $Al(OH)_3$ and $Al(OH)_4^{-}$. Using Chivot's method, the graphic in Fig. 6 is obtained. For a pH of 7, the calculated solubility of bayerite at 70°C and the calculated solubility of boehmite at 100°C are very close: ~$10^{-6}$ mol of Al/L.

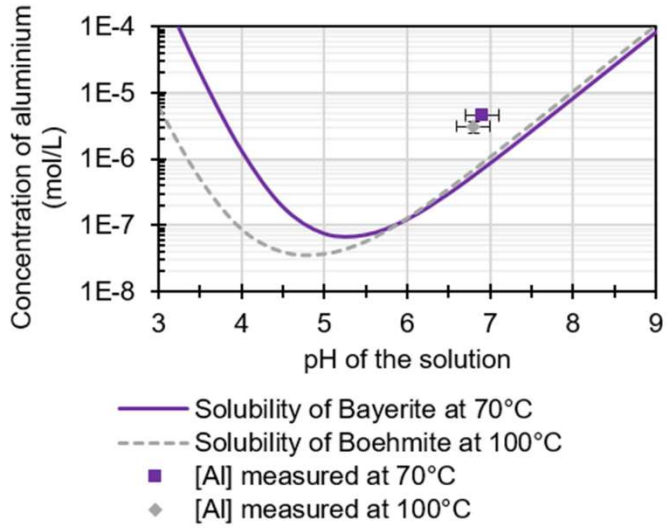


Figure 6: Calculated solubility of bayerite at 70°C and boehmite at 100°C according to the pH (Plotted from Chivot's calculation [39])

The two measured concentrations and the two calculated hydroxide solubility are very close at 70 and 100°C. As a result, other factors can explain the difference of aluminium corrosion between the two temperatures such as the different microstructure of the outer layer of the film at 70 and 100°C.

dioxygen solubility in solution: indeed, when the temperature increases, the dioxygen solubility decreases [15]. In this study, before corrosion tests, the dioxygen present in the atmosphere and in the solution is removed by injecting helium in autoclaves (cf. *Experimental Methodology*): the corrosive medium is deaerated. Because of this experimental protocol, no or very few dioxygen is present in the corrosive medium during corrosion tests. Moreover, the effect of dioxygen dissolved in solution on aluminium corrosion was studied by Hart [13]: for a temperature above 70°C, no effect of dissolved dioxygen was observed. Thus, the corrosion difference observed between 70 and 100°C cannot be explained by a difference of dioxygen solubility.

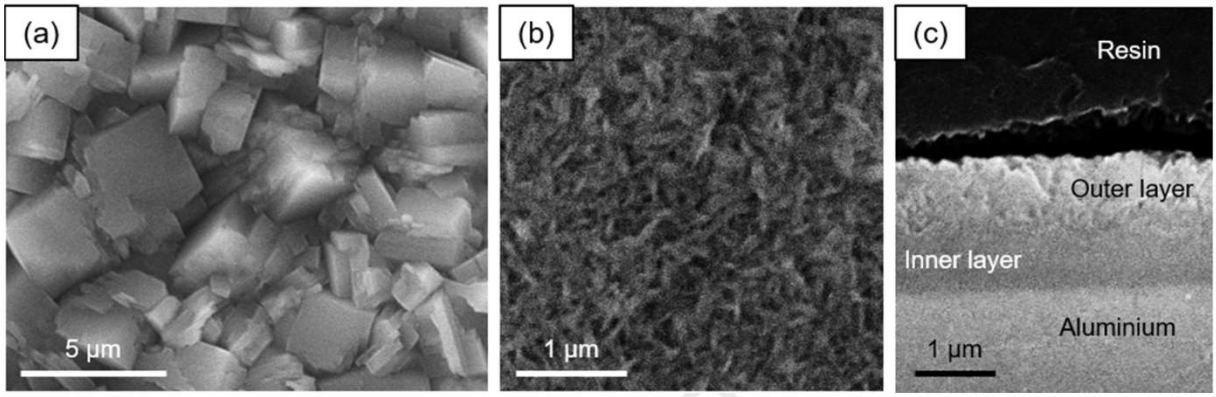


Figure 7: Micrographs (SEM, secondary electron mode) of the outer layer on the surface of the samples at (a) 70°C and (b) 100°C and (c) of a cross section of the hydroxide film at 100°C, obtained after corrosion test for 33 days in 0.065L of solution at initial pH 6.

Due to the change of the hydroxide phases at 70/80°C, the sample are more corroded at low temperature (70°C) than at high temperature (100°C) and the thickness of the hydroxide varies significantly between the two temperatures. These observations reveal the importance to complete the data used to develop the hydroxide thickness prediction models presented in the introduction: the empirical correlations between hydroxide thicknesses, testing time and condition of corrosion (temperature, pH, flow rate and heat flux) used in MTRs cannot be extrapolated at low temperature (70°C). In order to improve the data used for these models at low temperature, a parametric study is performed with different values of pH.

### 3.2.2 Effect of pH on uniform and localised corrosion

PH variations are observed during aqueous corrosion tests with aluminium alloys [15,16]. In this study, two volumes of solution are used: 0.065L and 2.8L. The large volume (2.8L) minimizes the variations of pH by a dilution effect. On the contrary, in the small volume (0.065L), since the corrosion of the AA-6061-T6 causes pH variations, it will be easier to observe the pH variations and to study its influence on aluminium corrosion. The corrosion tests are performed at 70°C and with an initial pH of 5.
After the corrosion tests, the pH is measured and presented in Fig. 8. In 0.065L, the pH increases from 5 to 7.5 on average and a dispersion of the points is observed. In the larger solution volume (2.8 L)

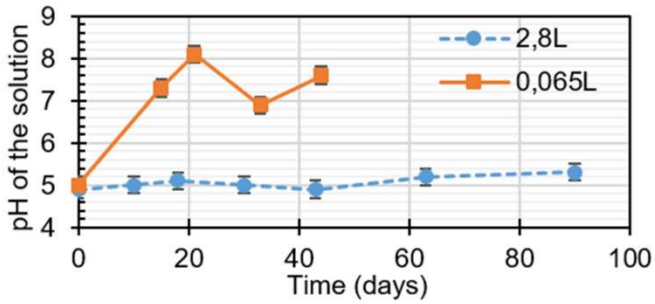


Figure 8: Evolution of the pH in two volumes of solution 0.065L and 2.8L at 70°C.

The Fig. 9 presents (a) the depth of pits and (b) the thickness of the film associated to uniform corrosion. The pits are deeper on average in 0.065L than in 2.8L. The depth is constant in time for long time of immersion (65 and 90 days in 2.8L). The formation of solid iron oxide and aluminium hydroxide gradually passives pits and stops their growth. The thickness of the inner layer of the film is constant with time in both volumes. The thickness of the outer layer is higher on average in 0.065L of solution with an average pH of 7.5 than in 2.8L of solution with a pH of 5 despite a dispersion of the points in 0.065L. The samples are therefore more corroded at an average pH of 7.5 than at a pH of 5. This observation is similar to the one made by Pawel et al. during corrosion tests at 105-208°C [4]. However, this study shows that at 70°C, the two layers do not have the same behaviour depending on the pH: the pH has an impact on the outer layer but not on the inner layer.

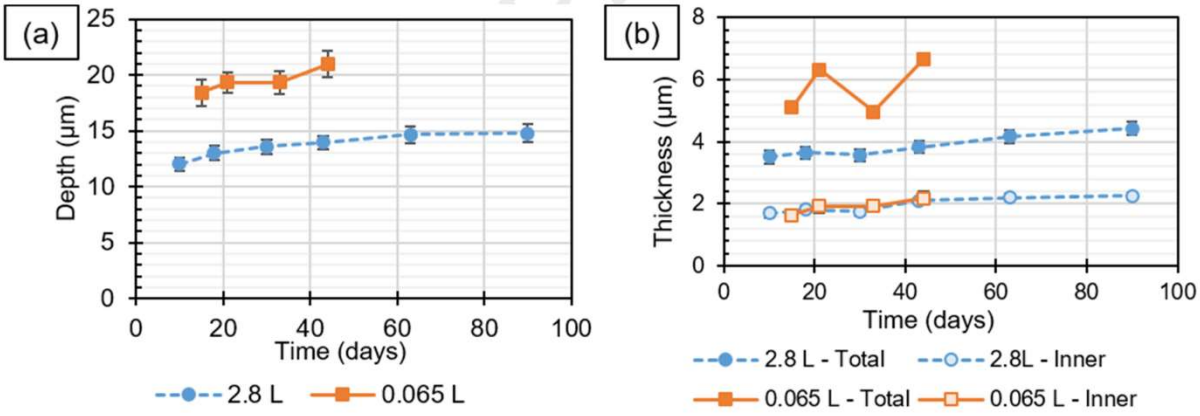


Figure 9: Evolution of (a) the average depth of pits and (b) the average total thickness of the film and the average thickness of the inner layer at 70°C in two volumes of solution 0.065L and 2.8L with an initial pH of 5.

In order to better understand the impact of the pH on the outer layer of the film, the surface of the samples corroded in the small volume 0.065L is observed using a SEM. The Fig. 10 presents different micrographs of pits on the surface of the samples for different times and final pH values. An effect of the final pH is observed on the microstructure of pits, on the hydroxide ring morphology. For 15 and 33 days (Fig. 10.a and c), a ring of hydroxide crystals surrounds the iron-rich inclusion. The ring

Therefore, the increase of pH causes an expansion of the ring surrounding the iron-rich inclusion until localised corrosion and uniform corrosion cannot be identified as separate forms of corrosion on the surface of the samples.

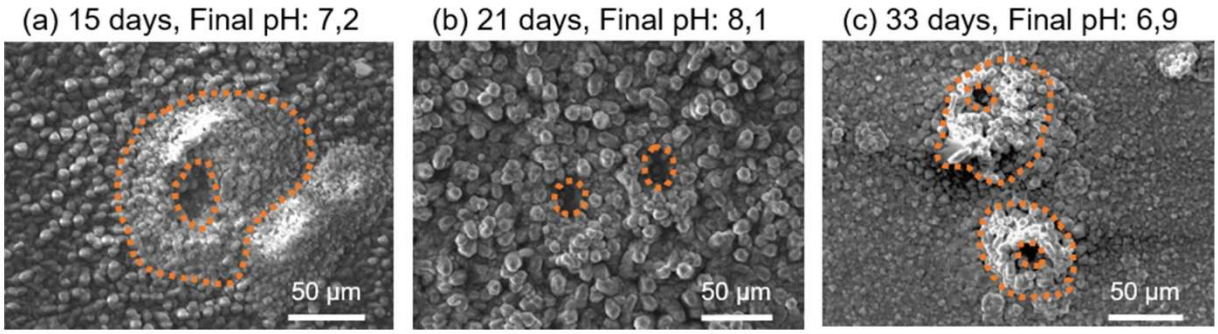


Figure 10: Micrographs (SEM, secondary electron mode) of pits of aluminium hydroxide on the surface of the samples in 0.065L of solution at 70°C for (a) 15 days, (b) 21 days and (c) 33 days.

## 4. DISCUSSION: PH VARIATIONS

The pH variations have an important impact on aluminium corrosion: because of these variations, the samples are more corroded in the small volume of solution. In order to better understand these variations, in this part, chemical reactions involved in the corrosion of the alloy 6061-T6 are proposed and their implication on the pH variations is discussed.

### 4.1.1 Corrosion reactions of the 6061-T6 alloy:

In tests performed without samples at 70°C, for 33 days and in 0.065L of solution, the pH is constant at 5. The variations are therefore due to the corrosion of the alloy AA-6061-T6 and are not due to the experimental materials. Before the corrosion tests, in the autoclave, the medium is deaerated, therefore, only the chemical species linked to water are taken into account in this study.

The iron-rich inclusions are corroded to form magnetite ($Fe_3O_4$) according to the examinations presented in the Section 3.1.1. After the corrosion tests, iron is not detected in the solution. The stability of magnetite instead of iron aqueous ions is due to the absence of dioxygen in the medium [32]. The mechanisms of magnetite formation were studied by Schikorr [40] :

$Fe_{(s)} + 2\ H_2O_{(l)} \rightarrow Fe(OH)_2 + \ H_{2(g)}$ (Reaction 1)

$3\ Fe(OH)_{2)} \rightarrow Fe_3O_{4(s)} + H_{2(g)} + 2\ H_2O$ (Reaction 2)

The corrosion of the inclusions does not induce pH variations according to reactions (1) and (2).

Corrosion of the $Mg_2Si$ particles leads to a release of ions $Mg^{2+}$ in solution and to the formation of the oxide $SiO_2$ (cf. section 3.1.2). In the pH domain of this experiment, the reaction of the oxidation of these particles is:

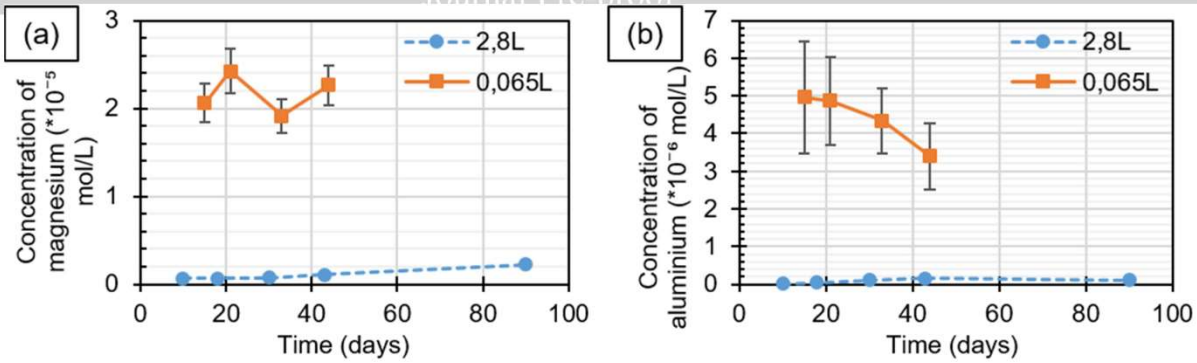


Figure 11: Evolution of the concentration of (a) magnesium and (b) aluminium in two volumes of solution, 0.065L and 2.8L, at 70°C.

According to the examinations performed on the samples (cf. section 3.1.3), the aluminium corrosion is described by the following reactions:

$Al_{(s)} + 2\ H_2O_{(l)} \rightarrow \gamma\text{-}AlOOH_{(s)} + 3/2\ H_{2(g)}$ (Reaction 4)

$Al_{(s)} + 3\ H_2O_{(l)} \rightarrow \alpha\text{-}Al(OH)_{3(s)} + 3/2\ H_{2(g)}$ (Reaction 5)

The corrosion mechanisms leading to the formation of the inner layer (boehmite) and the outer layer (bayerite) have been proposed by Wintergerst et al. [3]. These two reactions (4) and (5) do not induce pH variations. However, for a pH above 5, dissolution of the aluminium hydroxide occurs following the reaction [39]:

$\alpha\text{-}Al(OH)_{3(s)} + OH^-_{(aq)} \leftrightarrow Al(OH)_4^-{}_{(aq)}$ (Reaction 6)

The concentration of aluminium measured in the solution is presented in the Fig. 11.b for the two volumes of solution 0.065L and 2.8L. As the release of magnesium in solution and the dissolution of the aluminium hydroxide could cause pH variations, more calculations are needed.

#### 4.1.2 Corrosion of the $Mg_2Si$ particles and pH variations:

With the reaction (3), the $pH_{final}$ is calculated using the magnesium concentration $[Mg^{2+}]$ measured in solution. The quantity of material $n(OH^-)_{produced}$ of hydroxyl groups produced with the reaction (3) is :

$2\ n(OH^-)_{produced} = n(Mg^{2+})$ (Equation 7)

With $n(Mg^{2+})$ the quantity of material of magnesium measured in solution. The concentration $[OH^-]$ depends on the pH according: $[OH^-] = 10^{pH-pKe}$ with pKe the ionic product of water. The value of pKe is 12.804 at 70°C [41]. The Equation (8) and (9) are obtained:

$[OH^-]_{final} = [OH^-]_{initial} + [OH^-]_{produced}$ (Equation 8)

$[OH^-]_{final} = 10^{pHinitial-pKe} + ½ * [Mg^{2+}] = 10^{pHfinal\ -pKe}$ (Equation 9)

The final pH calculated is:

$pH_{final} = pKe + \log(\ ½ * [Mg^{2+}] + 10^{pHinitial-pKe})$ (Equation 10)

The final pH calculated with Eq. (10) and the pH measured in solution is presented in Fig. 12 in the two volumes of solution 0.065L and 2.8L and at 70°C. The pH measured and calculated correspond: their values are similar despite a dispersion of the measured points. Thus, the pH variations are mainly

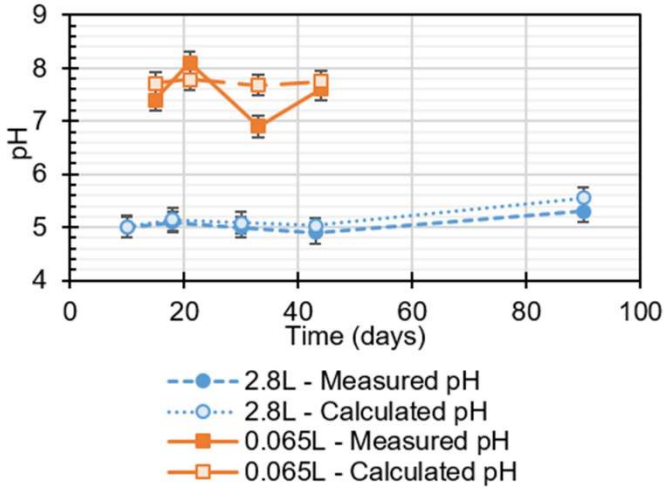


Figure 12: Evolution of the measured pH and the pH calculated with the Eq. (9) in two volumes of solution, 0.065L and 2.8L, at 70°C.

#### 4.1.3 Dissolution of the aluminium hydroxide and pH variations:

The pH variations modify the stability of the aluminium hydroxide according to reaction (6). The chemical equilibrium of precipitation/dissolution of aluminium hydroxide is determined by the solubility of bayerite. This solubility depends on pH and temperature. Fig. 13.a presents the solubility of bayerite at 70°C calculated by Chivot [39]. The aluminium concentration measured during the corrosion tests in 0.065L and 2.8L are also reported in Fig. 13.a. According to Fig. 13.a, an increase of pH from 5 to 8 causes an increase of the solubility and thus, an increase of the concentration of ions Al(III). According to Wintergerst et al. [3], the outer layer of the hydroxide film is formed by precipitation of ions Al(III) on the surface of the samples. The increase of solubility with the pH has a strong impact on the precipitation of ions Al(III) and thus on the outer layer. Fig. 14.b presents the evolution of thickness of the outer layer as a function of the final pH. Regardless of corrosion time and volume of solution, this thickness increases linearly with pH. According to the observations of the microstructure of pits on the surface of the samples in 0.065L in Section 3.2.2, at a pH of 8, the outer layer is formed by ions Al(III) released in solution by uniform corrosion and by localised corrosion: the ions Al(III) released by pits precipitate uniformly over the surface of the samples and cause the increase of the thicknesses of the outer layer. In addition, in 0.065L, a dispersion of the measured thicknesses of the outer layer is observed (Fig. 9.b), this dispersion corresponds to the pH variations.

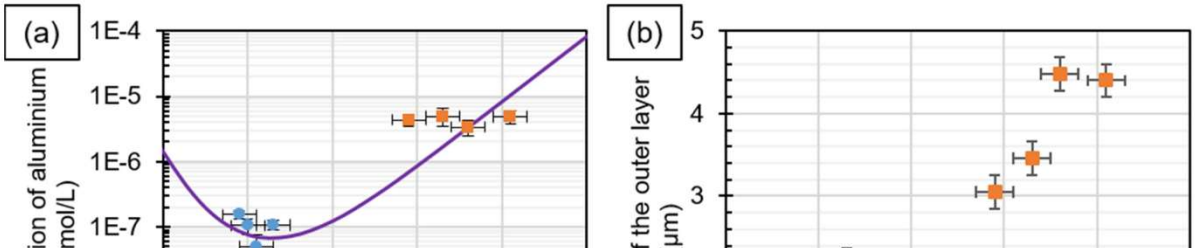

Figure 13: (a) Concentrations of aluminium measured in the two volumes, 0.065L and 2.8L, and solubility of bayerite calculated by Chivot [39] depending on the pH, and (b) thickness of the outer layer of the film depending of the final pH in the two volumes, 0.065L and 2.8L at 70°C.

The corrosion of the $Mg_2Si$ particles results in a release of magnesium in solution and an increase of pH. In 2.8L, due to a dilution effect, pH variations are negligible. On the contrary, in 0.065L, the concentration of magnesium increases a lot and causes an increase of pH. In the absence of magnesium in the alloy, pH variations should not be observed. When magnesium is released and pH increases, the solubility of the aluminium hydroxide increases, the film is less stable and the sample are more corroded. This observation is confirmed by a higher depth of pits in 0.065L of solution at a pH of 7.5 than in 2.8L of solution at a pH of 5.

#### 4.1.4 Verification of the origin of pH variations:

In order to verify the origin of the increase of pH, supplementary corrosion tests are performed. Coupons of pure aluminium and pure magnesium are immerged in 0.030L of solution (acid nitric diluted in pure water) at an initial pH of 5. The mass of the coupons is 0.2g. The coupons are corroded at 70°C (the tubes in Fig. 14.a and b are placed in incubator). A measure of the pH is regularly performed. Fig. 14.c presents the evolution of the pH. The coupon of pure aluminium is not dissolved (Fig. 14.a) and the pH is constant between 5 and 6. The coupon of pure magnesium is partially dissolved (Fig 14.b, the size of the coupon before the immersion was similar to the one of pure aluminium in Fig. 14.a) and the pH increases from 5 to 9 for 35 days. As a result, the increases of pH in the small volume of solution 0.065L is due to the release of magnesium in solution, to the corrosion of the $Mg_2Si$ particles for the 6061 aluminium alloy.

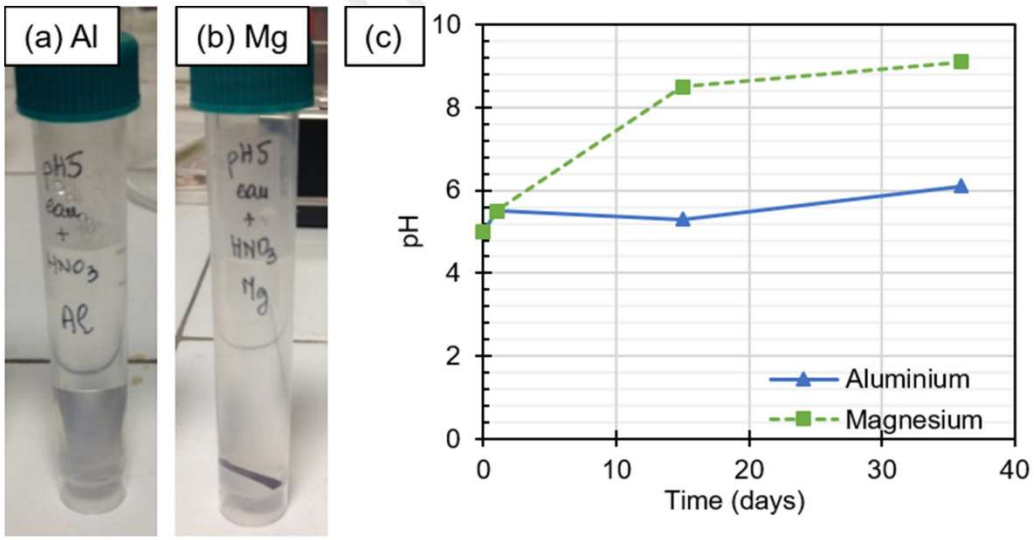


Figure 14: Tubes containing the coupons of (a) pure aluminium and of (b) pure magnesium and (c) evolution of the pH measured in the tubes at 70°C.

## CONCLUSIONS



In this study, corrosion tests are performed with various conditions on the aluminium alloy 6061-T6. Different parameters are tested: temperature 70 and 100°C) and pH. Each parameter has an important impact on localised and uniform corrosion.

. Both for localised and uniform corrosions, the samples are more corroded at 70°C than at 100°C. The hydroxide film shows a layered structure. The inner layer has the same microstructure and composition at the two temperatures. The outer layer appears to be very porous at 70°C: large gaps are present between hydroxide microcrystals. These gaps are not observed at 100°C. Due to their important size at 70°C, the gaps allow the aqueous solution to be directly in contact with the inner layer. As a result, the outer layer at 70°C is less protective for the aluminium alloy than the one at 100°C. At 70°C, the film is composed of two crystalline phases of aluminium hydroxide which have different properties (density, hydration and solubility) and the parameters of corrosion have not the same impact on each hydroxide. As a result, a distinction between the two layers needs to be done in the empirical correlations used to predict the hydroxide thickness in MTR. However, more corrosion tests at different temperatures inferior to 70°C are needed to adapt the coefficient of the empirical correlations.

In addition to the temperature, pH has a strong impact on aluminium corrosion. A pH of 5 limits aluminium corrosion compared to a pH of 7.5. This corrosion difference is due to the difference of solubility of aluminium hydroxide between the two pH: the high solubility at pH 7.5 decreases the stability of the film of aluminium hydroxide and thus, increases the aluminium corrosion. In addition, PH increase in a small volume of solution is due to the magnesium corrosion in deaerated medium. This oxidised magnesium comes from the micrometric $Mg_2Si$ particles. By releasing magnesium in solution, the corroded $Mg_2Si$ particles increasethe pH of the solution. The stability of aluminium hydroxides depends on the pH through their solubility. By increasing the pH, corrosion of the $Mg_2Si$ particles increase the solubility of aluminium hydroxides and thus, aluminium corrosion.

Pitting corrosion is due to the iron-rich intermetallic inclusions. After causing the formation of pits, the emerging iron-rich inclusions are corroded. This corrosion inhibits the pit growth for long time immersion and the depth of pits is constant with time. Thus the impact of pitting corrosion is less important than that of uniform corrosion and may not be taken into account in first order models of aluminium corrosion in MTR conditions when the 6061-T6 alloy is used for structures of nuclear core.

## ACKNOWLEDMENTS

This work received assistance from the “Agence Nationale de la Recherche” program GENESIS referenced as ANR-11-EQPX-0020.

## FIGURE CAPTIONS:

Figure 1: Micrograph of an aluminium hydroxide pit (SEM, secondary electron mode) and the corresponding dispersive X-rays spectroscopy of Al, O and Fe obtained after corrosion test at 70°C, for 30 day and in 2.8L of solution at pH 5.

Figure 2: µ-Raman pattern of an iron-rich inclusion located in the centre of an aluminium hydroxide pit, obtained after corrosion test at 70°C, for 30 day and in 2.8L of solution at pH 5.

Figure 3: Micrograph of $Mg_2Si$ particles (SEM, secondary electron mode) and corresponding dispersive X-rays spectroscopy of O, Mg and Si obtained after corrosion test at 70°C, for 30 day and in 2.8L of solution at pH 5.

Figure 4: (a) Micrograph of a cross section of the aluminium hydroxide film in bright field imaging (TEM), (b) µ-Raman pattern obtained on the the outer layer, and selected area electron diffraction patterns obtained from (c) the intermediate layer and (d) the inner layer (TEM); obtained after corrosion at 70°C, for 10 days in 2.8L of solution at a constant pH value of 5.

Figure 5: X-ray diffraction patterns obtained on the corroded samples surface at 70 and 100°C, for 33 days of corrosion and in 0.065L of solution at initial pH 6.

Figure 6: Calculated solubility of bayerite at 70°C and boehmite at 100°C according to the pH (Plotted from Chivot's calculation [39])

Figure 7: Micrographs (SEM, secondary electron mode) of the outer layer on the surface of the samples at (a) 70°C and (b) 100°C and (c) of a cross section of the hydroxide film at 100°C, obtained after corrosion test for 33 days in 0.065L of solution at initial pH 6.

Figure 8: Evolution of the pH in two volumes of solution 0.065L and 2.8L at 70°C.

Figure 9: Evolution of (a) the average depth of pits and (b) the average total thickness of the film and the average thickness of the inner layer at 70°C in two volumes of solution 0.065L and 2.8L with an initial pH of 5

Figure 10: Micrographs (SEM, secondary electron mode) of pits of aluminium hydroxide on the surface of the samples in 0.065L of solution at 70°C for (a) 15 days, (b) 21 days and (c) 33 days.

Figure 11: Evolution of the concentration of (a) magnesium and (b) aluminium in two volumes of

Figure 13: (a) Concentrations of aluminium measured in the two volumes, 0.065L and 2.8L, and solubility of bayerite calculated by Chivot [39] depending on the pH, and (b) thickness of the outer layer of the film depending of the final pH in the two volumes, 0.065L and 2.8L at 70°C.

Figure 14: Tubes containing the coupons of (a) pure aluminium and of (b) pure magnesium and (c) evolution of the pH measured in the tubes at 70°C.

## REFERENCES


[1] S.J. Pawel, G.L. Yoder, C.D. West, B.H. Montgomery, The development of a preliminary correlation of data on oxide groth on 6061 aluminium under ANS thermal-hydraulic conditions, ORNLTM-11517. (1990).

[2] J.C. Griess, H.C. Savage, T.H. Mauney, J.L. English, Effect of heat flux on the corrosion of aluminium by water. Part I : Experimental equipment and preliminary results, Oak Ridge, TN, USA, 1960.

[3] M. Wintergerst, N. Dacheux, F. Datcharry, E. Herms, B. Kapusta, Corrosion of the AlFeNi alloy used for the fuel cladding in the Jules Horowitz research reactor, J. Nucl. Mater. 393 (2009) 369–380. https://doi.org/10.1016/j.jnucmat.2009.06.003.

[4] S.J. Pawel, D.K. Felde, R.E. Pawel, Influence of coolant pH on corrosion of 6061 aluminium under reactor heat transfer conditions, Oak Ridge, TN, USA, 1995.

[5] J.C. Griess, H.C. Savage, T.H. Mauney, J.L. English, J.G. Rainwater, Effect of heat flux on the corrosion of aluminium by water. Part II : Influence of water temperature, velocity and pH on corrosion-product formation, Oak Ridge, TN, USA, 1961.

[6] CEA, E-den, A Nuclear Energy Divison Monograph, Les Réacteurs nucléaires expérimentaux, Le Moniteur, 2005.

[7] C. Vargel, Corrosion de l'aluminium, Dunod, 1999.

[8] J.C. Griess, H.C. Savage, T.H. Mauney, J.L. English, J.G. Rainwater, Effect of heat flux on the corrosion of aluminium by water. Part III : Final report on tests relative ot the high-flux isotop reactor, Oak Ridge, TN, USA, 1961.

[9] Y.S. Kim, H.T. Chae, S.V. den Berghe, A. Leenaers, V. Kuzminov, A.M. Yacout, Aluminum cladding oxide growth prediction for high flux research reactors, J. Nucl. Mater. 529 (2020) 151926. https://doi.org/https://doi.org/10.1016/j.jnucmat.2019.151926.

[10] S.J. Pawel, G.L. Yoder, D.K. Felde, B.H. Montgomery, M.T. McFee, The corrosion of 6061 aluminium under heat transfer conditions in the ANS corrosion test loop, Oxid. Met. 36 (1991) 175–194.

[11] J.C. Griess, H.C. Savage, J.L. English, Effect of heat flux on the corrosion of alumnium by water. Part IV : Tests relative to the advanced test reactor and correlation with previous results, Oak Ridge, TN, USA, 1964.

[12] K. Wefers, C. Misra, Oxides and hydroxides of aluminium, ALCOA Laboratories, 1987.

[13] R.K. Hart, The formation of films on aluminium immersed in water, Trans Faraday Soc. 53 (1956) 1020–1025.

[14] Y.S. Kim, G.L. Hofman, A.B. Robinson, J.L. Snelgrove, N. Hanan, Oxidation of aluminum alloy cladding for research and test reactor fuel, J. Nucl. Mater. 378 (2008) 220–228. https://doi.org/10.1016/j.jnucmat.2008.06.032.

[15] J.O. Park, C.H. Paik, Y.H. Huang, R.C. Alkire, Influence of Fe-Rich Intermetallic Inclusions on Pit Initiation on Aluminum Allovs in Aerated NaCl. J. Electrochem. Soc. 146 (1999) 517–523.

[17] K.A. Yasakau, M.L. Zheludkevich, S.V. Lamaka, M.G.S. Ferreira, Role of intermetallic phases in localized corrosion of AA5083, Electrochem. METHODS Corros. Res. Sel. Pap. 9th Int. Symp. EMCR 2006 18-23 June 2006 Dourdan Fr. 52 (2007) 7651–7659. https://doi.org/10.1016/j.electacta.2006.12.072.

[18] Z. Li, C. Li, Z. Gao, Y. Liu, X. Liu, Q. Guo, L. Yu, H. Li, Corrosion behavior of Al–Mg2Si alloys with/without addition of Al–P master alloy, Mater. Charact. 110 (2015) 170–174. https://doi.org/10.1016/j.matchar.2015.10.028.

[19] M.A. Pech-Canul, R. Giridharagopal, M.I. Pech-Canul, E.E. Coral-Escobar, Corrosion Characteristics of an Al-1.78%Si-13.29%Mg Alloy in Chloride Solutions, in: 2012. https://doi.org/10.1002/9781118495292.ch61.

[20] C. Flament, J. Ribis, J. Garnier, T. Vandenberghe, J. Henry, A. Deschamps, Electron irradiation-enhanced core/shell organization of Al(Cr, Fe, Mn)Si dispersoids in Al–Mg–Si alloys, Philos. Mag. 95 (2015) 1–12. https://doi.org/10.1080/14786435.2015.1009959.

[21] C. Flament, J. Ribis, J. Garnier, Y. Serruys, F. Leprêtre, A. Gentils, C. Baumier, M. Descoins, D. Mangelinck, A. Lopez, K. Colas, K. Buchanan, P. Donnadieu, A. Deschamps, Stability of β″ nano-phases in Al-Mg-Si(-Cu) alloy under high dose ion irradiation, Acta Mater. 128 (2017) 64–76. https://doi.org/10.1016/j.actamat.2017.01.044.

[22] J. Yi, G. Wang, S. Li, Z. Liu, Y. Gong, Effect of post-weld heat treatment on microstructure and mechanical properties of welded joints of 6061-T6 aluminum alloy, Trans. Nonferrous Met. Soc. China. 29 (2019) 2035–2046. https://doi.org/10.1016/S1003-6326(19)65110-1.

[23] S.K. Kairy, P.A. Rometsch, C.H.J. Davies, N. Birbilis, On the Electrochemical and Quasi In Situ Corrosion Response of the Q-Phase (AlxCuyMgzSiw) Intermetallic Particle in 6xxx Series Aluminum Alloys, CORROSION. 73 (2016) 87–99. https://doi.org/10.5006/2249.

[24] S.K. Kairy, T. Alam, P.A. Rometsch, C.H.J. Davies, R. Banerjee, N. Birbilis, Understanding the Origins of Intergranular Corrosion in Copper-Containing Al-Mg-Si Alloys, Metall. Mater. Trans. A. 47 (2016) 985–989. https://doi.org/10.1007/s11661-015-3296-3.

[25] T. Petit, J. Besson, C. Ritter, K. Colas, L. Helfen, T.F. Morgeneyer, Effect of hardening on toughness captured by stress-based damage nucleation in 6061 aluminum alloy, Acta Mater. 180 (2019) 349–365. https://doi.org/10.1016/j.actamat.2019.08.055.

[26] Y. Shen, Comportement et endommagement des alliages d'aluminium 6061-T6 : approche micrométrique, Thèse de doctorat, Ecole Nationale Supérieure des Mines de Paris, 2012.

[27] O. Lunder, B. Olsen, K. Nisancioglu, Pre-treatment of AA6060 aluminium alloy for adhesive bonding, Int. J. Adhes. Adhes. 22 (2002) 143–150. https://doi.org/10.1016/S0143-7496(01)00049-5.

[28] D.L.A. de Faria, S. Venâncio Silva, M.T. de Oliveira, Raman microspectroscopy of some iron oxides and oxyhydroxides, J. Raman Spectrosc. 28 (1997) 873–878. https://doi.org/10.1002/(SICI)1097-4555(199711)28:11<873::AID-JRS177>3.0.CO;2-B.

[29] C.J. Doss, R. Zallen, Raman studies of sol-gel alumina: Finite-size effects in nanocrystalliine AlO(OH), Phys Rev B. 48 (1993) 626–637.

[32] H.D. Ruan, R.L. Frost, J.T. Kloprogge, Comparison of Raman spectra in characterizing gibbsite, bayerite, diaspore and boehmite, J. Raman Spectrosc. 32 (2001) 745–750. https://doi.org/10.1002/jrs.736.

[33] G.G. Christoph, C.E. Corbato, D.A. Hofmann, R.T. Tettenhorst, The crystal structure of boehmite, Clays Clay Miner. 27 (1979) 81–86.

[34] A. Christensen, M. S. Lehmann, P. Convert, L. Beyer, O. Bastiansen, G. Braathen, L. Fernholt, G. Gundersen, C. J. Nielsen, B. N. Cyvin, S. J. Cyvin, Deuteration of Crystalline Hydroxides. Hydrogen Bonds of gamma-AlOO(H,D) and gamma-FeOO(H,D), Acta Chem. Scand. - ACTA CHEM SCAND. 36 (1982) 303–308. https://doi.org/10.3891/acta.chem.scand.36a-0303.

[35] R.T. Downs, M. Hall-Wallace, The American Mineralogist Crystal Structure Database, Am. Mineral. 88 (2003) 247–250.

[36] R. Rothbauer, F. Zigan, H. O′Daniel, Verfeinerung der Struktur des Bayerits, Al(OH)3, Z. Für Krist. - Cryst. Mater. 125 (2015) 317. https://doi.org/10.1524/zkri.1967.125.16.317.

[37] R.W.G. Wyckoff, Crystal structures, Arizona. Wiley (Interscience), University of Arizona, Tucson, 1965. https://doi.org/10.1016/0003-9861(65)90258-4.

[38] J. Chivot, Solubilité de la boehmite et de la bayérite et spéciation de l'aluminium en solution aqueuse en fonction du pH et de la température, CEA/FAR - CEREM, 1997.

[39] I.-W. Huang, B.L. Hurley, F. Yang, R.G. Buchheit, Dependence on Temperature, pH, and Cl− in the Uniform Corrosion of Aluminum Alloys 2024-T3, 6061-T6, and 7075-T6, Electrochimica Acta. 199 (2016) 242–253. https://doi.org/10.1016/j.electacta.2016.03.125.

[40] G. Schikorr, Zeitschrift für Anorganishe und Allgemeine Chemie, (1933) 212.

[41] International Association for the Properties of Water and Steam, Revised Release on the Ionization Constant of H2O, (2019). http://www.iapws.org/relguide/Ionization.pdf.

**Declaration of interests**

☒ The authors declare that they have no known competing financial interests or personal relationships that could have appeared to influence the work reported in this paper.

☐The authors declare the following financial interests/personal relationships which may be considered as potential competing interests: